Taylor & Francis
Taylor & Francis Group

Exploration Geophysics

ISSN: 0812-3985 (Print) 1834-7533 (Online) Journal homepage: https://www.tandfonline.com/loi/texg20

Adapting the use of AEM for greenfields VHMS exploration under cover

Andrea Viezzoli, Antonio Menghini, Nicholas Ebner & Paul Hilliard

To cite this article: Andrea Viezzoli, Antonio Menghini, Nicholas Ebner & Paul Hilliard (2019): Adapting the use of AEM for greenfields VHMS exploration under cover, Exploration Geophysics, DOI: 10.1080/08123985.2019.1667733

To link to this article: https://doi.org/10.1080/08123985.2019.1667733

Published online: 07 Oct 2019.

https://doi.org/10.1080/08123985.2019.1667733

Adapting the use of AEM for greenfields VHMS exploration under cover

Andrea Viezzoli[a], Antonio Menghini[b], Nicholas Ebner[c] and Paul Hilliard[d]

[a]Aarhus Geophysics Aps, Voldbjergvej, Risskov, Denmark; [b]Aarhus Geofisica Srl, Via Giuntini, Cascina (PI), Italy; [c]Newexco Services Pty Ltd, Joel Terrace, East Perth, Western Australia; [d]Sandfire Resources NL, Kings Park Road, West Perth, Western Australia

ABSTRACT

Electromagnetics (EM) has been used extensively for Volcanic Hosted Massive Sulphide (VHMS) exploration in Australia. Exploring under conductive cover introduces significant limitations when using EM to identify bedrock conductivity anomalies that may be associated with VHMS deposits. We present an alternative approach, whereby robust geological modelling of the Airborne Electromagnetic (AEM) data plays a major role in the exploration strategy in the Bryah and Yerrida Basins of central Western Australia. The AEM is not only used for the identification of bedrock conductors but also forms a critical dataset constraining a robust basin-wide geological model. This model is used to identify priority areas for follow up surface geophysics and geochemistry. A patchwork of AEM surveys, covering portions of the Bryah and Yerrida basins, has been acquired by various explorers and contractors during the last decade. Systems and system specifications vary greatly. Accordingly, accurate geological interpretation of a basin-scale area, flown using various systems, cannot be derived from either raw data or fast/approximate conductivity products provided by contractors. All datasets require reconciliation with a common workflow and robust modelling strategy. Historic AEM data acquired with different systems along the edges of the tenure have been reprocessed and inverted. The remaining central block awaits the contractor's arrival before the data is subject to the same workflow. The end result will be a seamless basin-wide 3D conductivity model (extending over 6500 km^2), which will inform the geological interpretation and subsequent follow-up exploration efforts. The preliminary 3D models already allow clear identification and modelling of the pyritic shale horizons, enabling the anomalous geochemistry and strongly conductive nature of these units to be discounted in the targeting process

ARTICLE HISTORY
Received 4 September 2018
Accepted 15 July 2019

KEYWORDS
3D modelling; airborne electromagnetics; case histories; exploration methodologies; mineral exploration; interpretation

Introduction

Mineral exploration in the Yerrida and Bryah basins is hampered by extremely poor exposure, deep weathering and palaeochannel cover. Geochemical analyses of surface samples on a regional scale has produced strong metal and pathfinder anomalies that, based on evaluation drilling by previous explorers, have been demonstrated to be associated with continuous (stratigraphic) disseminated pyrite in carbonaceous shales. No economically significant mineralisation has been identified in the pyritic shales and as such the strong geochemical anomalies from these units must be discounted. Given the poor exposure and low stratigraphic contrast in aeromagnetic response, previous geological interpretations of the Yerrida basin have failed to accurately domain areas within which pyritic shales occur. This has led to repeated unsuccessful historic exploration campaigns. One of the key contributions expected of the AEM is the mapping of the pyritic shale horizons. Another is the identification of paleochannels infilled with fine grained clay-rich material such that appropriate exploration methods can to be adopted in these areas.

Sandfire Resources NL is the owner of several AEM datasets (Figure 1) collected over a 10 year timeframe (2009–2018), using different systems: HeliTEM^{TM} (Smith, Hodges, and Lemieux 2009), VTEM^{TM} (Witherly, Irvine, and Morrison 2004) and Xcite^{TM} (Combrinck and Wright 2016).

For the analysis of the geophysical results, we referred to the Sandfire Resources NL 1:250′000 scale regional interpretation of the Bryah and Yerrida basins (Figure 2). The structural architecture of the project area comprises a periclinal anticline (the Goodin Dome) bounded to the north and south by synclines. Subsequent to the folding, a series of ENE-WSW striking faults developed, juxtaposing stratigraphic units of different ages, in the vicinity of the Gascoyne River.

In order to justify the approach presented in this paper, the AEM data is first presented as maps of voltage values. This is where exploration companies often stop, looking merely for the anomalous responses at late times. Figures 3 and 4 show the voltage (pV/Am^4), at selected times after turn-off, recorded by the 5 AEM surveys across the tenure. We chose, from all systems, "early time" gates closest to $\sim$ 150 μs and the "mid-

CONTACT Andrea Viezzoli av@aarhusgeo.com Aarhus Geophysics Aps, Voldbjergvej 14A, Risskov, 8240, Denmark

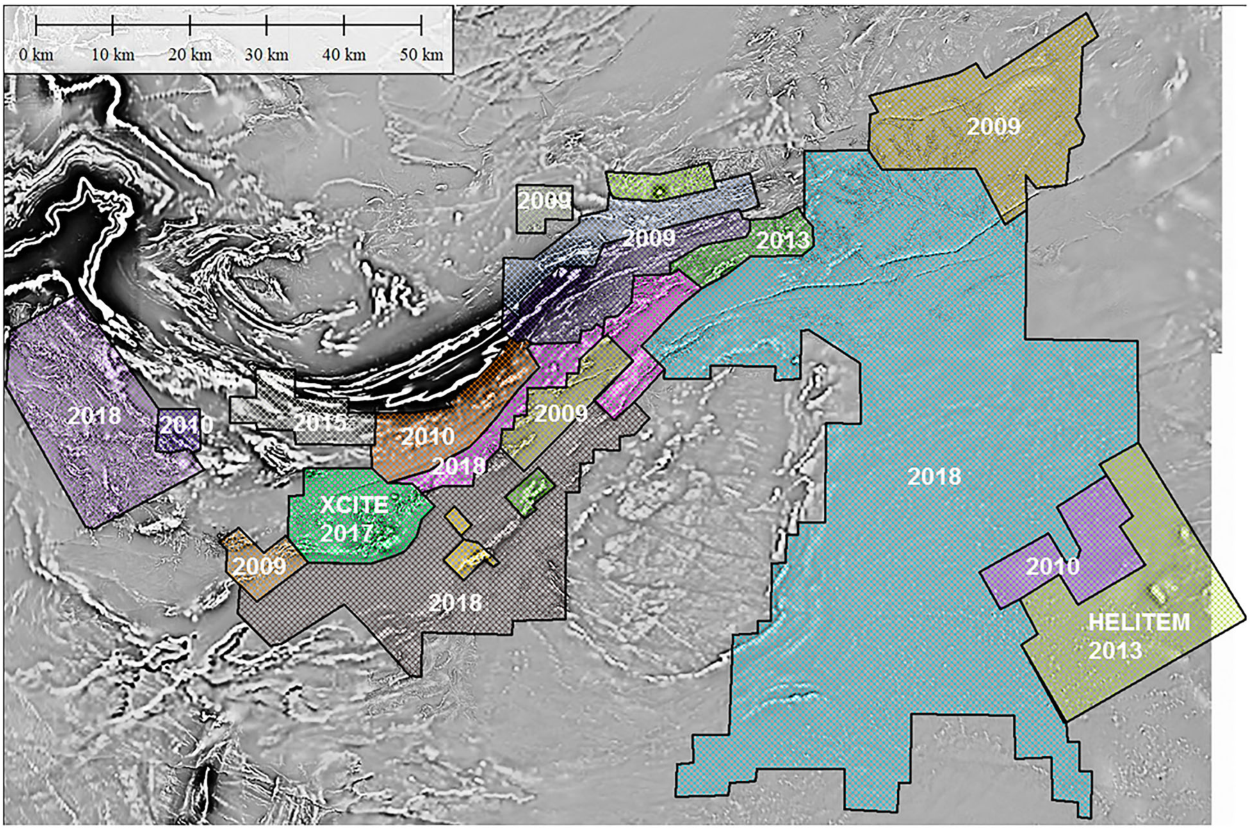

Figure 1. First vertical derivative (reduced to pole) aeromagnetic image of the Bryah and Yerrida basins showing the extent of different AEM surveys conducted over the area. Where not specified the acquisition system was VTEM. The 2018 survey areas were planned during the preparation of this communication.

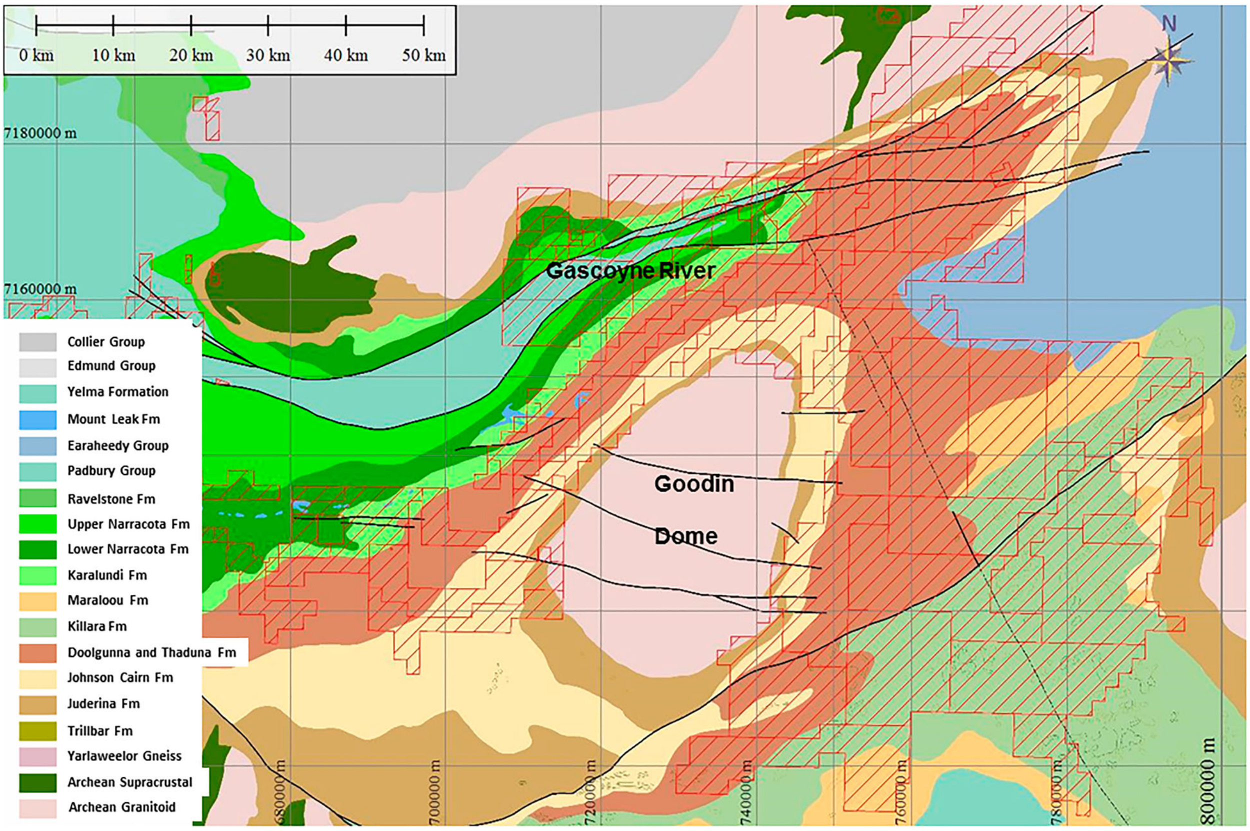

Figure 2. Regional geological interpretation of the Yerrida and Bryah basins based on regional geological mapping (Geological Survey of Western Australia 1981, 1985), aeromagnetic imagery and drilling. This interpretation was completed prior to development of the current AEM model. The red hatched areas show exploration tenement areas.

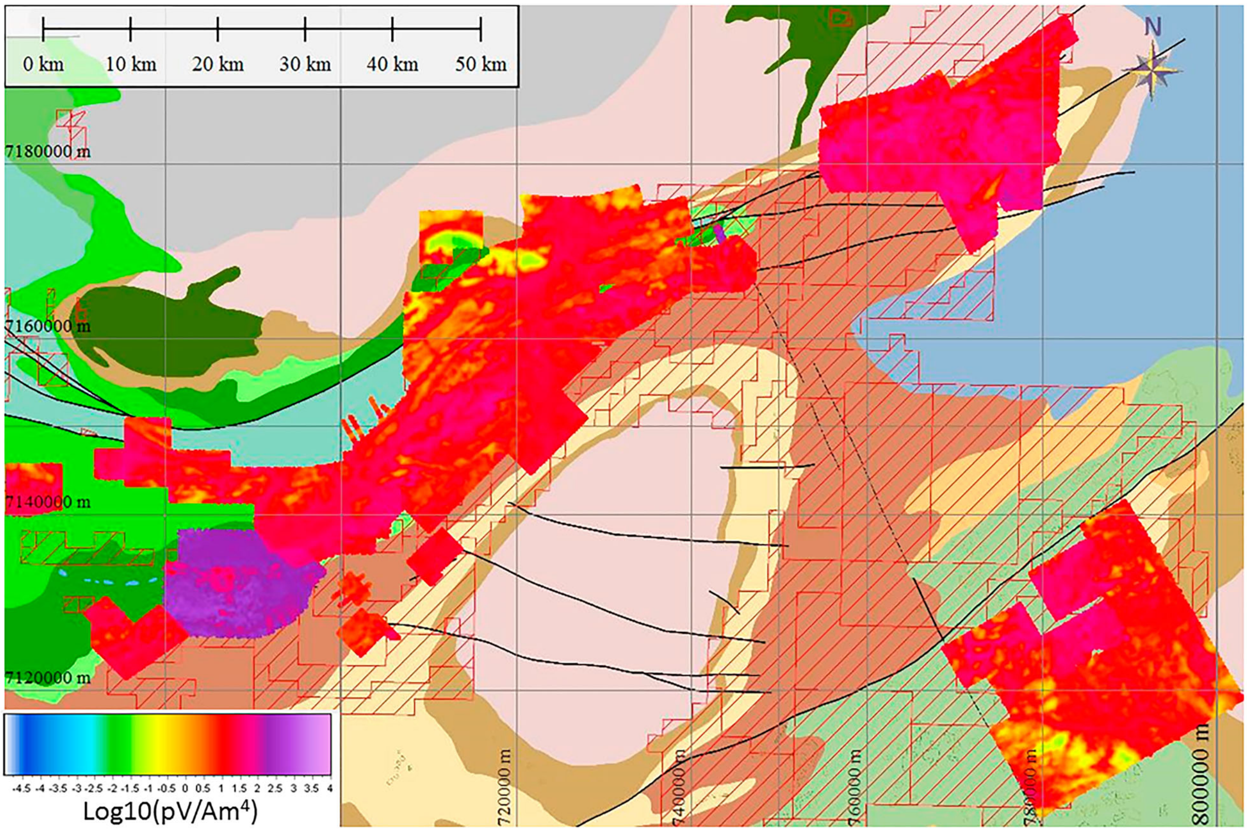

Figure 3. Voltage response (pV/Am^4) imagery for the historic AEM surveys for early time-gate (± 150µs) draped on the geological interpretation.

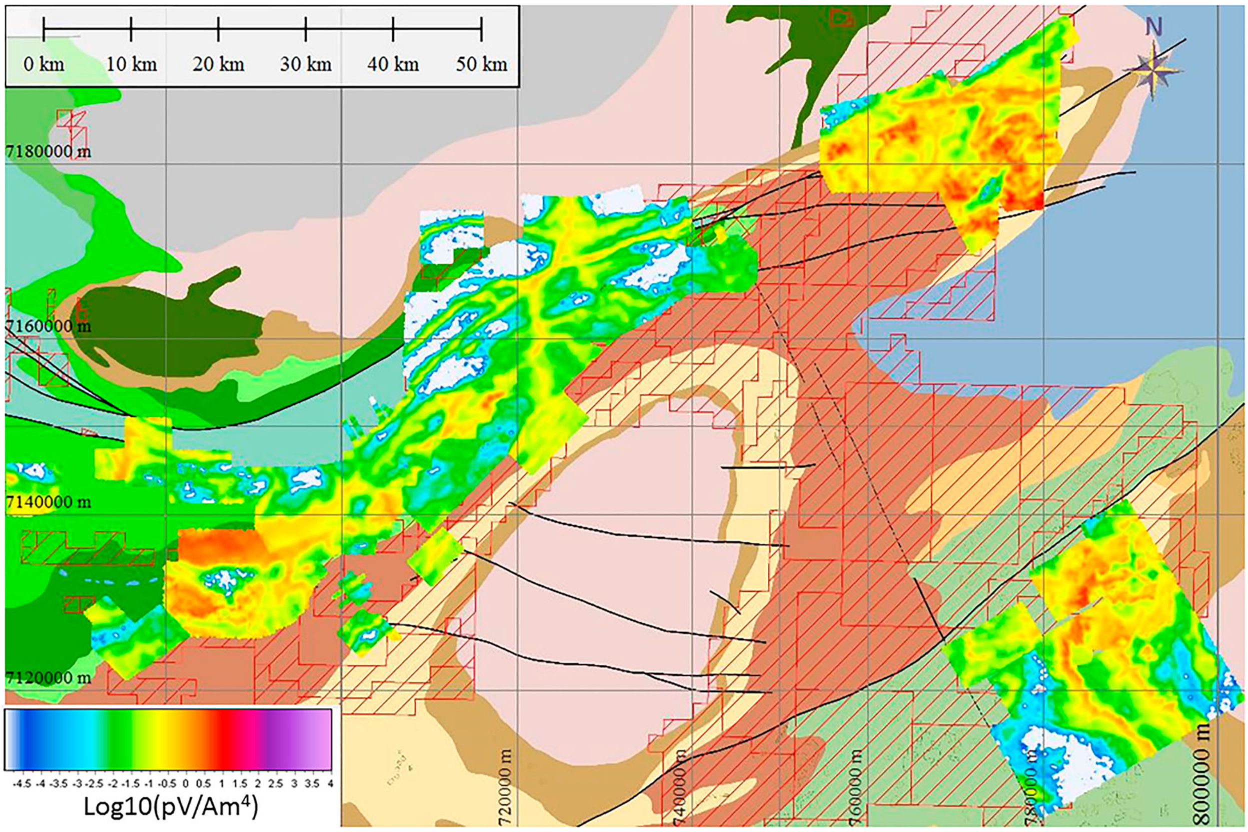

Figure 4. Voltage response (pV/Am4) imagery for the historic AEM surveys at mid-late time gate (± 3ms) draped on the geological interpretation. White coloured areas represent negative values (possible IP effects).

Table 1. System parameters for different AEM systems historically deployed in the Yerrida and Bryah basins.

AEM system	Transmitter loop area (m^2)	Number of turns	Trasmitter Current (A)	Dipole moment (Am^2)	Gate times range (ms)
HeliTEM	708	2	1415	2,000.000	0.156–14.258
Xcite	265.9	4	220	233,996	0.0091–12.49
VTEM	531	4	180–209	382,320–444,000	0.083–10.667

late time" gates at ~3 ms (both from the end of ramp). Obvious system dependent features in the data – for example, normalisation by the effective moment does not remove the waveform shape from the system transfer function – hinder seamless merging. Figures 3 and 4, whilst showing that significant geological complexity is reflected in the data, do not allow understanding of the 3D variability of the conductivity, nor the causative geological sources. The requirement to reduce the size of the exploration search-space prompted an effort to extract as much information as possible from the AEM data.

The existing datasets

Since the different datasets come from different airborne systems, evaluation of the relevant system specifications was essential prior to developing a processing and interpretation work-flow. The system specific features need to be taken into account when modelling and visualising the data. The Xcite data (Figures 1 and 3) for example, has a higher early time signal due to its faster ramp down compared with that of the other systems deployed in the area.

The systems all had a base frequency of 25 Hz. Waveforms were either trapezoid or sinusoidal, and dipole moments differed by almost an order of magnitude (Table 1). The duty cycles ranged from ~ 30% to ~ 45% and the number of gates varied from ~20 to ~ 50. The first gate time covered a spread from ~ 20 μs to > 100 μs and the duration of transmitter current ramp down ranged from ~ 100 μs to in > 2 ms.

Methods

The role of data processing is crucial for AEM, especially when merging datasets from different acquisition systems. Processing and inversion was completed one dataset at a time, although it was envisaged that the results would be eventually merged into a seamless model for geological interpretation.

Accurate modelling of AEM data first requires a true description of the system transfer function (STF) for each system. Failure to properly describe the STF (waveforms, gate-times, filters, transmitter geometry, receiver geometry etc) can introduce serious artefacts in the inversions.

For the purpose of this study, each of the actual digital waveforms was closely and evenly sampled,

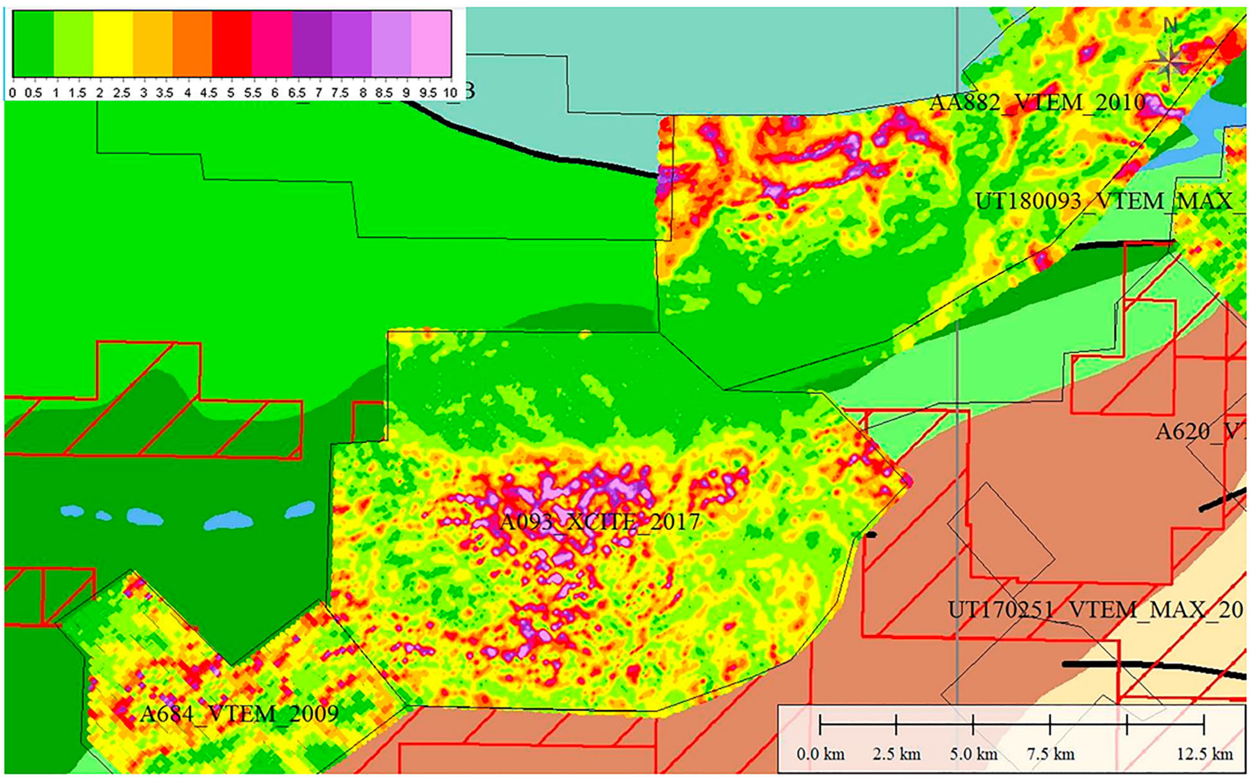

Figure 5. Map of a portion of the study area showing misfit values for 3 of the survey areas draped on the geological interpretation.

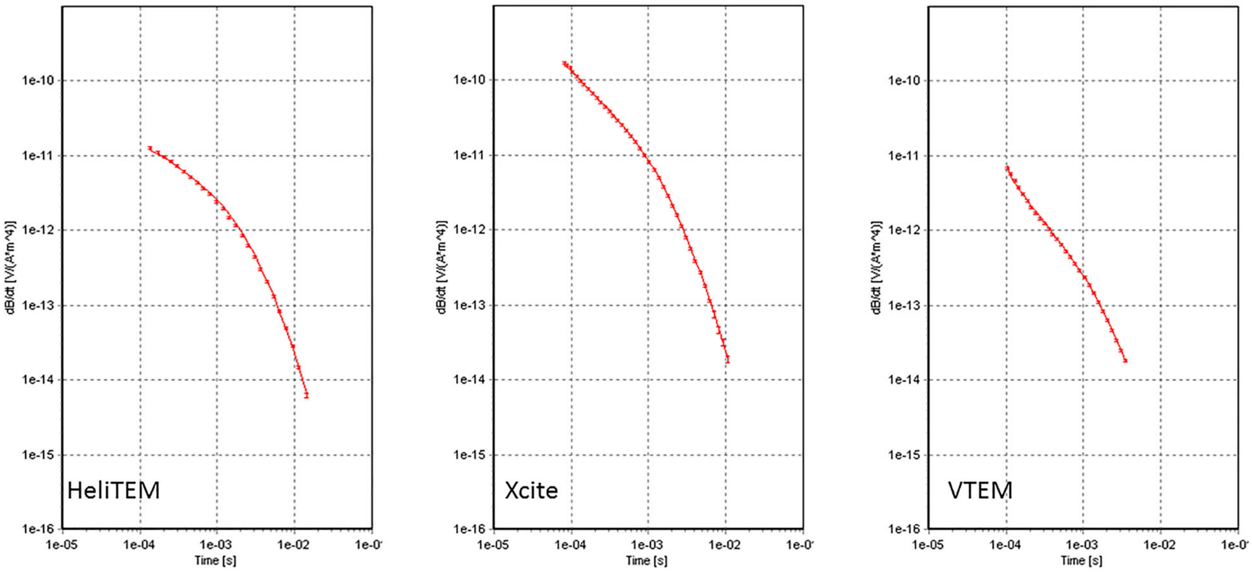

Figure 6. Examples of data fitting of forward responses. From the left: HeliTEM, Xcite and VTEM surveys.

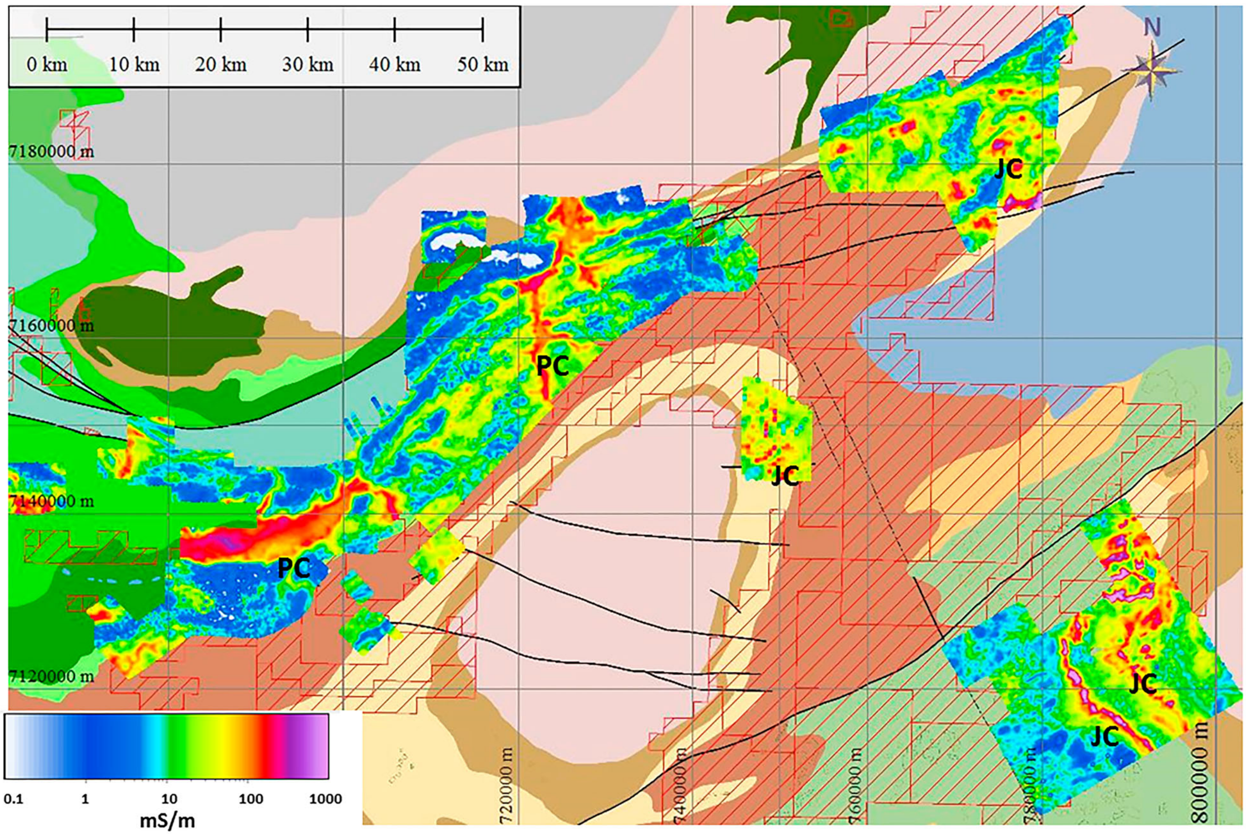

Figure 7. Plan view of a 40–50m depth slice of the conductivity model, draped on the geological interpretation. PC = Palaeochannel, JC = Pyritic Johnson Cairn shale.

down to the end of ramp-down. These often differed significantly from the nominal waveforms. The EM and navigation data were then custom processed, starting from the rawest dataset available (i.e. with lowest amount of pre-processing by the contractors). The processing protocol utilised both automated and manual editing, to obtain the best balance between signal/noise whilst preserving lateral resolution (Auken et al. 2009).

Noisy gates were either culled or had their uncertainty increased. It is important to note that the noise measured by an AEM system is not constant across a survey. Applying a constant noise floor underestimates its value in places and overestimates it in others. This translates into either artefacts or loss of information in the deeper parts of the derived conductivity models.

Full non-linear inversion (based on exact 1D forward solution, L1 norm) with spatially constrained inversion

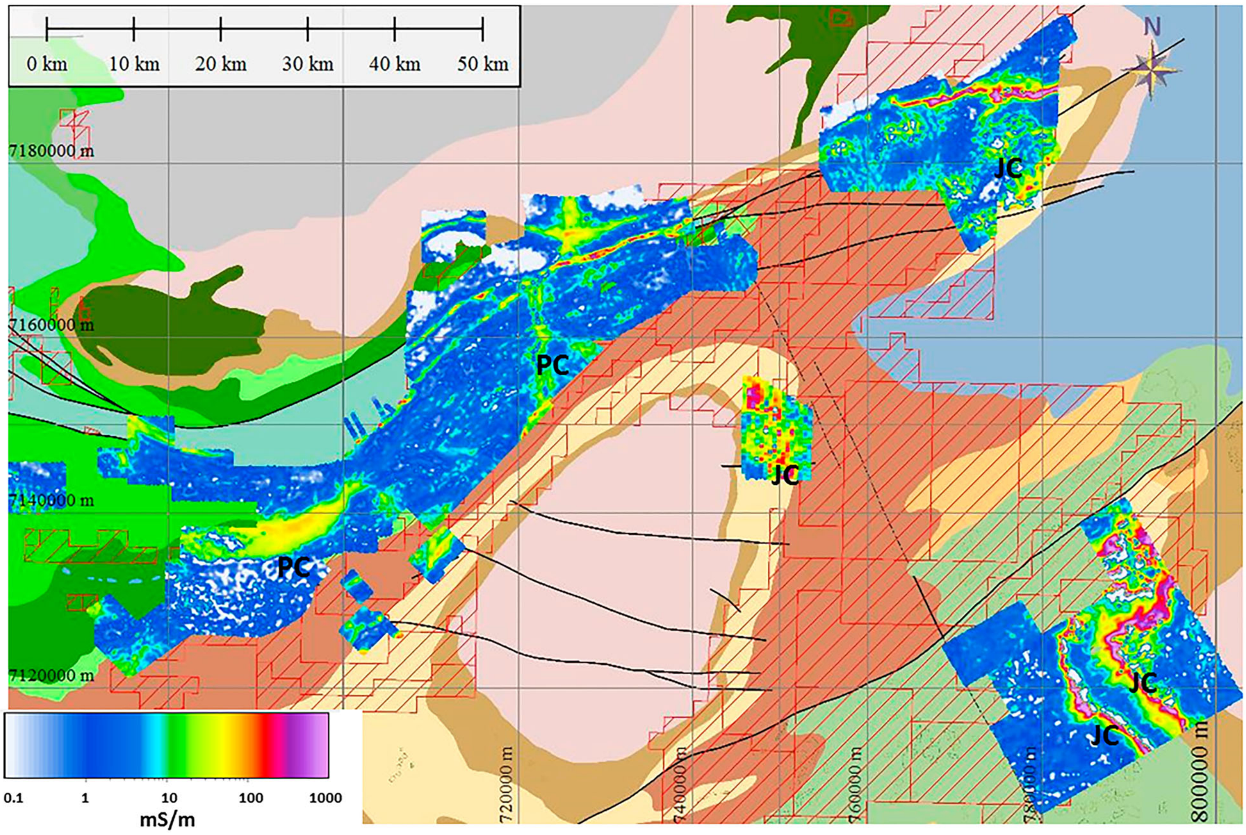

Figure 8. Plan view of a 100–120m depth slice of the conductivity model, draped on the geological interpretation. PC = Palaeochannel, JC = Pyritic Johnson Cairn shale.

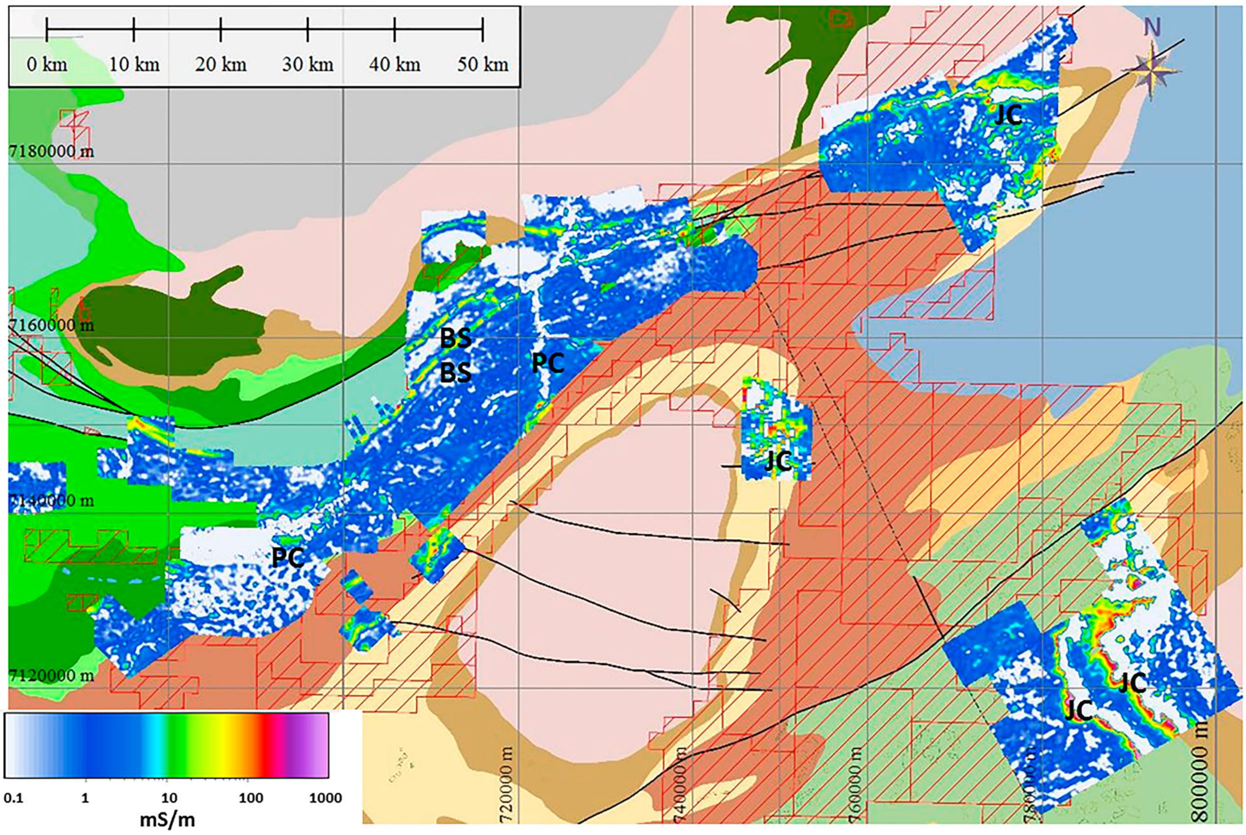

Figure 9. Plan view of a 200–220m depth slice of the conductivity model, draped on the geological interpretation. PC = Palaeochannel, JC = Pyritic Johnson Cairn shale, BS = Pyritic Padbury Group shale.

("SCI"; Viezzoli et al. 2008) was then undertaken. The inversion code was AarhusInv (Kirkegaard and Auken 2015). The SCI improves the robustness of the inversion results by exploiting the expected geological spatial coherence. Numerous preliminary inversions with different regularisation settings were completed on each dataset, and the results compared with available geological information. Care was taken to avoid smearing laterally the anomalies d ue to excessive regularisation. Through this iterative process a common setting was selected and applied to all blocks for the final inversions, carried out separately for each dataset.

The multi-layered model used fixed thicknesses discretised into 30 layers; however, the resistivity value of each layer remains a free parameter to be fit during the inversions. The model depth was restricted to 700 m, with layers logarithmically increasing in thickness and in resistivity: the upper most (shallow) layer starting at 5 m, with 20 Ωm, the deepest at 700 m, and 300 Ωm. Both the vertical and horizontal constraints are intended to be loosely constrained, so as to allow sharp variations in the resistivity models.

Depth of Investigation ("DOI"; Christiansen and Auken 2012) was calculated on each dataset, and the results accordingly cropped. The DOI is a crucial metric, as it allows portions of the models to be identified that are characterised by low sensitivity and a high probability of inversion artefacts. By cropping the data at the DOI, geological interpretation can be restricted to portions of the model that have a high confidence.

The data misfit for each transient was determined and is considered satisfactory, averaging $\sim$ 3 for all surveys. There is a considerable variability in the data misfit (Figure 5) as one would expect from surveys covering a large and geologically heterogeneous area. Strong 3D effects and locally improvable inversion settings (i.e. starting models) can cause anomalous misfit. The data misft does not show abrupt changes along dataset boundaries.

It is also recognised that there are Airborne Induced Polarization (AIP) effects in part of the AEM data that can be identified by change of polarity in the measured transients and very fast decays. The AIP effects were not modelled at this stage and the negatives were simply deleted. It should be noted that this treatment of AIP effects can cause local high misfits and of potential artefacts in the derived resitivity model (Viezzoli, Kaminski, and Fiandaca 2017). In particular, underestimation of depth to resistive bedrock.

Examples of transients with measured and modelled data for different systems are shown in Figure 6.

Subsequent to inversion of each data set the inversion results were then merged into a common resistivity model that was used for the geological interpretation. Overlapping or neighbouring portions of surveys were

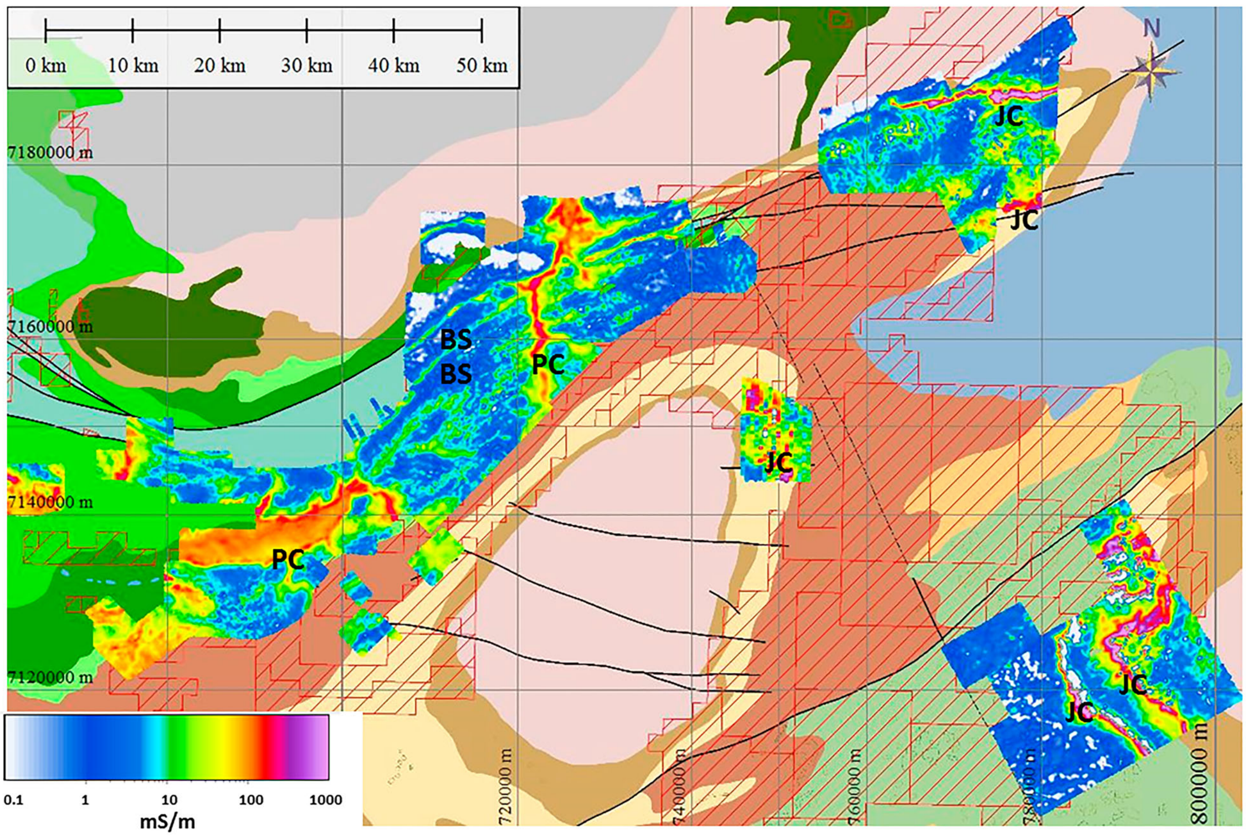

Figure 10. Image of the 3-D model at elevation of 400–490 metres above sea-level draped on the geological interpretation. PC = Palaeochannel, JC = Pyritic Johnson Cairn shale, BS = Pyritic Padbury Group shale.

compared and this confirmed that the methodology applied yielded virtually seamless models.

Results

Maps, cross sections and 3D conductivity voxels were derived from the common model. Figures 7–9 illustrate conductivity slices at different depths. The new 3D models allow clear identification and modelling of the pyritic shale horizons that occur within the Johnson Cairn Formation and Padbury Group. These pyritic shale horizons occur as discrete markers beds with the host formation and the strongly conductive nature is not characteristic of the entire stratigraphic unit. These are the only demonstrably conductive formations within the Proterozoic bedrock. Low conductivity lithotypes include sandstone, dolomite, conglomerate, greywacke, siltstone, dolerite, basalt, gneiss and granite.

Further conductive domains are present in the Quaternary palaeochannel cover, particularly where they have a primary silt or clay composition. Although groundwater in much of the area is non-saline, decreased resistivity in alluvial sand or gravel due to presence of saline groundwater cannot be excluded. It has also been noted that, locally, lateritic and pisolitic cover have imparted IP effects on the AEM data.

Figure 7 shows the conductive response of two large paleochannels (PC), one spatially coincident with the current Gascoyne river (Figure 2), whilst the south-western one is spatially coincident with the Murchison River. The conductive features imaged on the eastern side of the study area (Figure 7) are coincident with pyritic shale layers within the Johnson Cairn Formation (JC). The conductive structures follow geological contacts consistent with the regional structural framework and are thus stratigraphic in nature. The map pattern of the sulphidic shales in the south-eastern part of the study area is well resolved in Figure 7 but that in the north-eastern survey is less clear due to overlying palaeochannel cover.

At greater depth (Figure 8), the Johnson Cairn pyritic shales in the north-eastern part of the study are are better imaged. Cross-cutting ENE-WSW striking faults have displaced the sulphidic shale units in both the north-eastern and south eastern areas giving the conductors a fragmented appearance in areas so affected. Portions of the Gascoyne and Murchison palaeochannels are imaged showing considerable thicknesses of paleochannel cover in these areas.

Figures 8 and 9 show ENE-WSW striking conductors that relate to sulphidic shales (BS) in the Padbury Group (Figure 2) that sub-outcrop in the axial region of a syncline. The Padbury Group is a late Proterozoic sequence that, in this area, has been juxtaposed against older Bryah Group strata by ENE-WSW striking faults.

The 200–220 m depth slice (Figure 9) shows large blanked (cropped) areas indicating that the DOI has been exceeded. The map pattern of the Johnson Cairn Formation black shales is well resolved. The impact of Gascoyne and Murchison palaeochannels on the DOI is also evident.

An image of the model at an elevation of 490–500 m above mean sea level (Figure 10) provides a clearer view of the aforementioned geological features without the influence of current topography on depth to sub-surface geology.

As illustrated in Figure 11 there are substantial disconnects between the pre-existing geological interpretation and the model developed from the AEM. These disconnects reflect the poor constraints available for the geological interpretation (limited outcrop available for surface mapping and the small amount of lithostratigraphic magnetic susceptibility contrast in aeromagnetic imagery). The AEM model can be used as an additional constraint to produce a robust geological and structural interpretation.

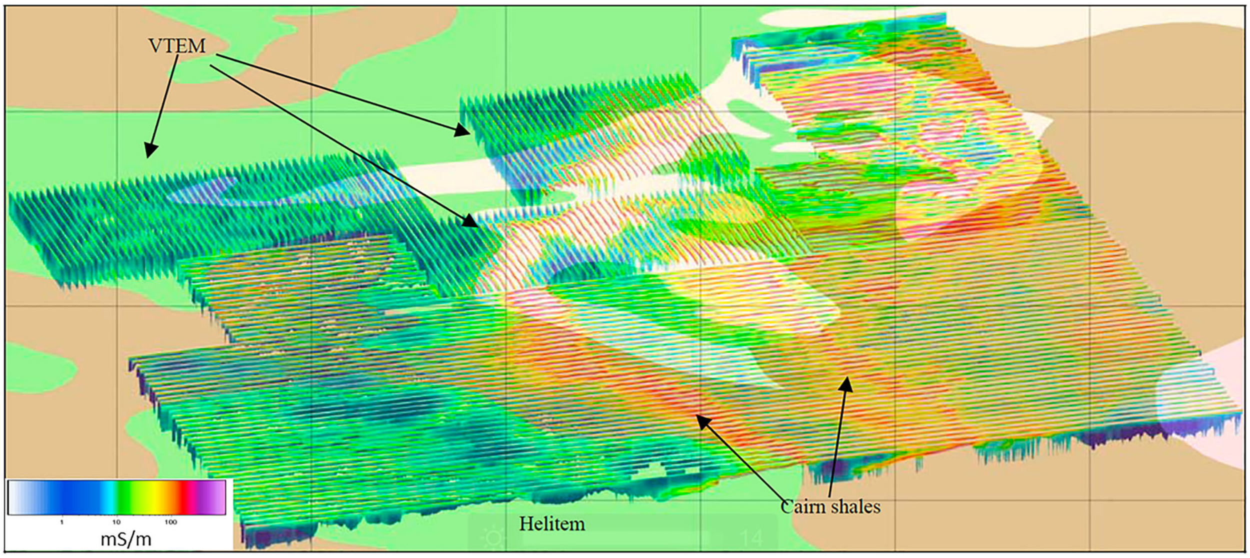

Figure 11. 3-D view of conductivity sections in the SE portion of the study area, draped on the pre-existing geological interpretation.

The advanced modelling and derived interpretation will allow conductive reponses and coincident geochemistry of the pyritic shale units to be discounted in the targeting process. Discrete conductors with more subtle geochemical responses, in prospective stratigraphy, can be identified and evaluated.

The new model also allows geometry and depths of palaeochannel cover to be determined. Whilst the conductivity of the basement below the highly conductive palaeochannels is rarely well resolved, the modelling process allows appropriate exploration methods (drilling for geochemical samples and downhole electromagnetic surveys) to be adopted in palaeochannel covered areas.

Neither the geometry of the pyritic shale horizons, nor that of the paleochannels could have been resolved by merging of the data/deliverables provided by AEM contractors. The processing work-flow presented here has provided a step-change in the quality of geological interpretation.

Conclusions

Reprocessing and inversion of a patchwork of historic AEM surveys over a large tenement holding in Western Australia will result in the generation of a seamless basin-wide conductivity model. The development of this model was made possible through the amalgamation of data from a number of exploration projects and emphasises the value of taking a regional approach to exploration.

Based on the results of this approach, litho-stratigraphic boundaries have been redefined, and understanding of the structural framework has increased significantly. Exploration search space has been narrowed and focussed and the targeting of "false" positives associated with discrete conductive sediments has been eliminated. The planning of future exploration programs in the presence of thick palaeochannel sequences has been refined substantially. This focussing of the exploration was particularly important, as it was achieved in tenement areas with very weak litho-stratigraphic magnetic susceptibility contrasts, which would otherwise significantly encumber the exploration effort.

This level of interpretation would arguably not have been achieved without a rigorous approach to processing and inversion replacing the simple data transforms often used for geological interpretation of AEM data. A more detailed examination of the results will provide crucial information for future exploration activity.

Disclosure statement

No potential conflict of interest was reported by the authors.

References

Auken, E., A.V. Christiansen, J.H. Westergaard, C. Kirkegaard, N. Foged, and A. Viezzoli. 2009. An integrated processing scheme for high-resolution airborne electromagnetic surveys, the SkyTEM system. *Exploration Geophysics* 40: 184–92.

Christiansen, A.V., and E. Auken. 2012. A global measure for depth of investigation. *Geophysics* 77, no. 4: WB171–7.

Combrinck, M., and R. Wright. 2016. Xcite™: Great results require more than good data. *ASEG-PESA, 2016, Adelaide, Australia*.

Geological Survey of Western Australia. 1981. Geological Series, Glengarry sheet, scale 1:250,000, SG 50–12.

Geological Survey of Western Australia. 1985. Geological Series, Peak Hill sheet, scale 1:250,000, SG 50–8.

Kirkegaard, C., and E. Auken. 2015. A parallel, scalable and memory efficient inversion code for very large-scale airborne electromagnetics surveys. *Geophysical Prospecting* 63: 495–507.

Smith, R.S., G. Hodges, and J. Lemieux. 2009. Case histories illustrating the characteristics of the HeliGEOTEM system. *Exploration Geophysics* 40: 246–56.

Viezzoli, A., A.V. Christiansen, E. Auken, and K. Sorensen. 2008. Quasi-3D modeling of airborne TEM data by spatially constrained inversion. *Geophysics* 73, no. 3: F105–13.

Viezzoli, A., V. Kaminski, and G. Fiandaca. 2017. Modeling induced polarization effects in helicopter time domain electromagnetic data: synthetic case studies. *Geophysics* 82, no. 2: E31–50.

Witherly, K., R. Irvine, and E.B. Morrison. 2004. The Geotech VTEM time domain helicopter EM system. *SEG Expanded Abstract* 23: 1217–21.